

# Antiferromagnetic topological insulators in heavy-fermion systems

Mohsen Hafez-Torbati<sup>1,\*</sup>

<sup>1</sup>*Department of Physics, Shahid Beheshti University, 1983969411, Tehran, Iran*

The cooperation of electronic correlation and spin-orbit coupling can stabilize magnetic topological insulators which host novel quantum phenomena such as the quantum anomalous Hall state also known as Chern insulator (CI). Here, we investigate the existence of magnetic topological insulators with antiferromagnetic (AF) order in heavy-fermion materials. Our analysis relies on the half-filled Kane-Mele-Kondo (KMK) model with the AF Kondo interaction  $J_K$  coupling the spin of itinerant electrons with a  $S = 1/2$  localized spin at each lattice site. We consider the Néel AF ordering with the local magnetization not only perpendicular ( $z$ -AF ordering) but also parallel ( $xy$ -AF ordering) to the honeycomb plane. We show that in the absence of an energy offset between the two sublattices of the honeycomb structure the system is always topologically trivial. There is a transition from the trivial  $xy$ -AF insulator ( $xy$ -AFI) to the trivial Kondo insulator (KI) upon increasing  $J_K$ . We unveil that an alternating sublattice potential can lead to the stabilization of the  $z$ -AFCI and the  $z$ -AF quantum spin Hall insulator ( $z$ -AFQSHI). We address the charge excitations in the bulk as well as at the edges of the KMK model. We provide a systematic comparison between the size of the charge gap in the AFCI in heavy-fermion materials and the size of the charge gap in the AFCI in transition-metal compounds. Our findings can guide the future experimental studies searching for AF topological insulators in novel class of systems which can survive up to higher temperatures.

## I. INTRODUCTION

Since the experimental discovery of the quantum anomalous Hall effect in thin films of the topological insulator  $(\text{Bi,Sb})_2\text{Te}_3$  doped with the transition-metal element Cr at temperatures below 30 mK [1] there has been a large interest to establish the effect in other systems and at higher temperatures [2, 3]. The higher temperature realization is essential not only for application of the dissipationless charge transport in spintronic technology but also to extend the possible experimental technique for a deeper understanding of the effect and its related phenomena. Using high-quality samples [4] and a modulation doping technique the Chern insulator phase is realized at temperatures up to 2 K [5]. This is still more than one order of magnitude smaller than the Curie temperature  $T_C \approx 30$  K of the material.

In order to omit the detrimental effect of the disorder and shift the quantization temperature of the Hall conductance towards the magnetic transition temperature of the material extensive research efforts have been dedicated in recent years to finding magnetic topological insulators which show intrinsic magnetic ordering [6, 7]. This has led to the theoretical prediction and experimental verification of multiple intrinsic magnetic topological insulators such as  $\text{MnBi}_2\text{Te}_4$  [8–14]. The existence of the Chern insulator [15] as well as the axion insulator [16] phase are confirmed in thin films of  $\text{MnBi}_2\text{Te}_4$  depending on the number of septuple layers being odd or even. Despite the remarkable development in the realization of the CI in an intrinsic magnetic topological insulator the reported quantization temperature is still limited to below 2 K [15]. This can be attributed to the negligible charge gap in the system [12–14].

The third class of systems in which the CI phase is observed is moiré materials. This includes twisted bilayer graphene

aligned to hexagonal boron nitride [17] and twisted transition metal dichalcogenide heterobilayers [18]. In contrast to the magnetically doped topological insulators a charge gap several times the Curie temperature is reported. However, the small Curie temperature  $T_C \approx 7$  K still limits the observation of the quantum anomalous Hall effect to only a few kelvins.

In all the above cases the stabilization of the CI is linked to the ferromagnetic nature of the material. Antiferromagnets, however, are much more common in nature in contrast to ferromagnets. They create no stray field, are robust against disturbing magnetic fields, and support a spin dynamics in the THz regime due to the large exchange interaction. These features have made AF materials particularly important for the construction of the next-generation spintronic devices [19–21]. The realization of an AFCI is more cumbersome than its ferromagnetic counterpart. This is because in a ferromagnetic state the time-reversal symmetry is truly broken, i.e., it would not be possible to compensate the effect of the time-reversal transformation by a space group operation. In an AF state, however, such a composite antiunitary symmetry can exist preventing a finite Chern number [22–24]. The AFCI is already reported for transition-metal compounds in single-orbital [22, 23] as well as multi-orbital [25] models and also in density functional theory calculations [24, 26].

In this paper we investigate the existence of two-dimensional AF topological insulators including both the AFCI and the AFQSHI in heavy-fermion systems. It is one of the main aims of this study to compare the size of the charge gap in the AFCI in heavy-fermion materials and in transition-metal compounds. Our analysis relies on the half-filled KMK model using the dynamical mean-field theory (DMFT) technique [27]. We consider the Néel AF ordering with the local magnetization not only perpendicular to the honeycomb plane ( $z$ -AF ordering) but also parallel to it ( $xy$ -AF ordering) comparing their energies. In the absence of an energy offset between the two sublattices of the honeycomb structure we show that the system is a trivial  $xy$ -AF insulator ( $xy$ -AFI) which undergoes a transition to the trivial Kondo insulator (KI) upon

\* [m.hafeztorbati@gmail.com](mailto:m.hafeztorbati@gmail.com)

increasing the Kondo interaction  $J_K$ . We uncover that introducing the alternating sublattice potential  $\delta$  can lead to the stabilization of both the  $z$ -AFCI and the  $z$ -AFQSHI. Complementary to the topological invariant calculations we confirm the existence of the gapless charge excitations localized at the edges for only one spin component in the AFI phase and also the closing of the bulk charge gap across the topological phase transitions. We provide a systematic comparison between the size of the charge gap in the AFI in heavy-fermion systems and the size of the charge gap in the AFI reported for transition-metal compounds [25].

The paper is organized as follows. In the next section we introduce the KMK model and discuss the technical aspects. In Sec. III we present the phase diagram of the KMK model in the  $J_K$ - $\delta$  plane. Sec. IV is devoted to a comprehensive study of the charge excitations in the system. The paper is concluded in the last section.

## II. MODEL AND METHOD

The KMK model serves as a paradigm for the study of the effect of the spin-orbit coupling in heavy-fermion systems [28–30]. The Hamiltonian of the model is given by

$$H = +t \sum_{\langle i,j \rangle} \sum_{\alpha} c_{i\alpha}^{\dagger} c_{j\alpha} + i\lambda_{\text{SO}} \sum_{[i,j]} \sum_{\alpha\beta} \nu_{ij} c_{i\alpha}^{\dagger} \sigma_{\alpha\beta}^z c_{j\beta} + \sum_i \sum_{\alpha} \delta_i c_{i\alpha}^{\dagger} c_{i\alpha} + J_K \sum_i \vec{s}_i \cdot \vec{S}_i, \quad (1)$$

where  $c_{i\alpha}^{\dagger}$  and  $c_{i\alpha}$  are the usual creation and annihilation fermionic operators at the honeycomb lattice site labeled by  $i$  and with the  $z$  component of the electron spin  $\alpha = \uparrow$  or  $\downarrow$ . The notation  $\langle i, j \rangle$  in the first term and the notation  $[i, j]$  in the second term limit sites  $i$  and  $j$  to be nearest-neighbor (NN) and next-nearest-neighbor, respectively. The first term in Eq. (1) is the NN hopping. The second term originates from the spin-orbit coupling with the honeycomb layer chosen in the  $x$ - $y$  plane.  $\sigma^z$  is the Pauli matrix and  $\nu_{ij} = 2/\sqrt{3}(\hat{d}_1 \times \hat{d}_2)_z = \pm 1$  with  $\hat{d}_1$  and  $\hat{d}_2$  being unit vectors along the two bonds the electron traverses going from site  $j$  to  $i$  [31]. We suppose  $\lambda_{\text{SO}} \geq 0$  without the loss of generality. The third term is an alternating sublattice potential giving the onsite energy  $\delta_i = +\delta$  to the sublattice  $A$  and the onsite energy  $\delta_i = -\delta$  to the sublattice  $B$  of the honeycomb structure. Such an alternating sublattice potential is extensively used to study transitions between topological and normal insulators [32–35] and also to realize AF topological states [22–24, 36, 37]. The alternating sublattice potential can be fine-tuned by applying a perpendicular electric field to a buckled structure [38, 39]. The last term in Eq. (1) is the AF Kondo interaction ( $J_K > 0$ ) coupling the electron spin  $\vec{s}_i$  to the localized spin  $\vec{S}_i$  with the size  $S = 1/2$  at each lattice site. The Hamiltonian is relevant for two-dimensional systems with a strong spin-orbit coupling and buckled structure such as silicene [40] grown on an appropriate magnetic insulating substrate [41]. The Heisenberg exchange interaction between the localized spins neglected in

Eq. (1) is not expected to have a substantial effect on our results except shifting the transition to the KI state to a larger Kondo coupling  $J_K$ .

The first three terms in Eq. (1) define the Kane-Mele model  $H_{\text{KM}}$  [31, 32]. For  $\delta < 3\sqrt{3}\lambda_{\text{SO}}$  the opposite spins carry the opposite Chern numbers  $\mathcal{C}_{\alpha} = \text{sgn}(\alpha)$  with  $\text{sgn}(\uparrow) = +1$  and  $\text{sgn}(\downarrow) = -1$  and the system describes a QSHI characterized by the spin Chern number  $\mathcal{C}_s = (\mathcal{C}_{\uparrow} - \mathcal{C}_{\downarrow})/2 = 1$ . Increasing the value of  $\delta$  the charge gap closes at  $\delta = 3\sqrt{3}\lambda_{\text{SO}}$  and a transition to the trivial band insulator phase with  $\mathcal{C}_{\alpha} = 0$  takes place. An infinitesimal Kondo interaction couples the electron spins to the localized spins and leads to the magnetic ordering due to the van Vleck mechanism [42, 43]. In the opposite limit that  $J_K$  is the dominant term the electron spin and the localized spin at each lattice site form a singlet state and the system becomes a paramagnetic KI.

The third interesting limit is the atomic limit for which  $t = \lambda_{\text{SO}} = 0$ . For  $\delta > 3J_K/4$  the sublattice with the lower onsite energy is fully occupied and the sublattice with the higher onsite energy is empty. For  $\delta < 3J_K/4$  each lattice site is occupied by one electron forming a singlet with the localized spin. These two states with completely different charge distributions become degenerate at  $\delta = 3J_K/4$ . Exotic quantum phases are expected to emerge around  $\delta = 3J_K/4$  upon introducing the hopping and the spin-orbit coupling.

To address the KMK model from weak to strong interaction limits we adopt the DMFT which is an established method for strongly correlated systems [27, 44] and is widely used to investigate the interplay of strong electronic correlation and spin-orbit coupling [23, 30, 34, 45–48]. The method fully takes into account the local quantum fluctuations but neglect non-local quantum fluctuations by approximating the self-energy to be spatially local,  $\Sigma_{ij;\alpha\beta}(i\omega_n) = \Sigma_{i;\alpha\beta}(i\omega_n)\delta_{ij}$ . The spin off-diagonal elements of the self-energy corresponding to  $\alpha \neq \beta$  are necessary to access solutions with a local magnetization out-of the  $z$  direction. Note that addressing these solutions are necessary for a proper analysis of the model as a finite spin-orbit coupling in Eq. (1) reduces the SU(2) symmetry to the U(1) symmetry. We employ the real-space realization of the DMFT [49–51] as it allows to capture not only the bulk but also the edge properties on equal footing. We specifically use the implementation introduced in Ref. 52 which is suitable for capturing different types of magnetic orderings. It is already applied to Kondo lattice models with [25] and without spin-orbit coupling [53, 54]. The lattice model is mapped to a set of effective Kondo impurity problems depending on the symmetry of the lattice. For bulk properties using periodic boundary conditions in both directions two Kondo impurity models are set up, one for sublattice  $A$  and one for sublattice  $B$ . In the absence of the sublattice potential  $\delta$  this can be reduced to one even in the Néel AF phase because the phase is still symmetric with respect to a combined swap of the sublattice and the spin orientation. To address edge properties we consider open boundary conditions in  $x$  and periodic boundary conditions in  $y$  direction (cylindrical geometry) treating the honeycomb structure as a brick wall shown in Fig. 1 with each lattice site labeled by two integers  $x$  and  $y$ . We have mainly used  $L \times L$  lattices

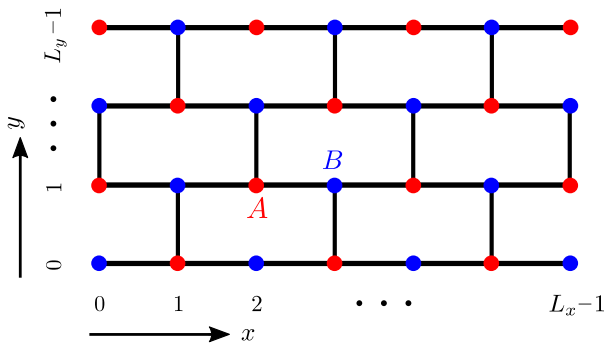


FIG. 1. The treatment of the honeycomb lattice as a brick wall. The number of lattice sites in the  $x$  direction is  $L_x$  and in the  $y$  direction is  $L_y$ . Each lattice site is identified by two integers  $(x, y)$ . The higher energy sublattice  $A$  and the lower energy sublattice  $B$  are specified.

with  $L = 40$  but we have produced data also for  $L = 60$  for selective points close to phase transitions making sure that the results are independent than the system size.

We opt for exact diagonalization (ED) [27, 55] to solve the Kondo impurity problem because it permits for a quantum mechanical treatment of the localized spin in contrast to the quantum Monte Carlo (QMC) solver which suffers from the fermionic sign problem and is restricted only to classical spins [56–58]. In addition, the ED solver provides a direct access to the real-frequency spectral function while in a QMC treatment an analytical continuation is required. Due to the finite number of bath sites in the ED solver the spectral function consists of separate sharp peaks which approximate a continuous function. However, the charge gap extracted from the ED spectral function is found accurate and is used to benchmark the results obtained from the QMC solver [59]. In view of a future finite temperature analysis we perform a full diagonalization for comparability. We provide data for different number of bath sites corroborating the accuracy of the results.

To distinguish distinct topological phases one needs to compute topological invariants, which is challenging for an interacting model. The topological invariant of an interacting system can be computed using twisted boundary conditions [60]. However, it requires access to the eigenstates of the Hamiltonian which is out of the DMFT scope. In the absence of a non-trivial ground state degeneracy, such as the one occurring in fractional quantum Hall effect, the topological invariant of an interacting system can be computed using the Ishikawa-Matsuyama formula which requires momentum and frequency integration over the Green's function and its derivatives [61–63]. Using an adiabatic deformation of the Green's function without the charge gap closing it is shown that only the zero-frequency Green's function is needed to determine the topological invariant of an interacting model [64]. The approach is called the topological Hamiltonian method. It relates the topological invariant of an interacting system to the topological invariant of an effective non-interacting model known as the topological Hamiltonian which in the second quantiza-

tion form is given by

$$H_{\text{top}} = H_0 + \sum_{ij} \sum_{\alpha\beta} c_{i\alpha}^\dagger \Sigma_{ij;\alpha\beta}(0) c_{j\beta} \quad , \quad (2)$$

where  $H_0$  stands for the non-interacting part of the original Hamiltonian and  $\Sigma_{ij;\alpha\beta}(0)$  is the self-energy at zero frequency.

The topological Hamiltonian approach should be used with caution. The derivation of the topological Hamiltonian (2) relies on the adiabatic deformation of the imaginary frequency Green's function such that it never becomes singular, i.e., the charge gap never closes. However, the Green's function and its inverse appear symmetrically in the Ishikawa-Matsuyama formula and the topological invariant can change not only if the poles but also if the zeroes of the Green's function occur [65]. The latter corresponds to the divergence of the self-energy and can be captured in our DMFT analysis.

In the DMFT approximation the self-energy is local. In the  $z$ -AF phase the self-energy in addition has no off-diagonal spin element,  $\Sigma_{i;\alpha\beta}(i\omega_n) = \delta_{\alpha\beta} \Sigma_{i;\alpha}(i\omega_n)$ , and is real at zero frequency. Using the symmetry  $\Sigma_{A;\alpha}(0) = -\Sigma_{B;\alpha}(0)$  between the zero-frequency self-energies on sublattices  $A$  and  $B$  the topological Hamiltonian simplifies to the Kane-Mele model with the effective spin-dependent alternating sublattice potential

$$\tilde{\delta}_\alpha = \delta + \Sigma_{A;\alpha}(0) \quad , \quad (3)$$

where  $A$  is the sublattice with the higher onsite energy. Using this relation one can easily determine the topological nature of a  $z$ -AF state. The system is in the  $z$ -AFQSHI if  $|\tilde{\delta}_\alpha| < 3\sqrt{3}\lambda_{\text{SO}}$  for both up and down spins, is in the  $z$ -AFCI if  $|\tilde{\delta}_\alpha| < 3\sqrt{3}\lambda_{\text{SO}}$  for one spin and  $|\tilde{\delta}_\alpha| > 3\sqrt{3}\lambda_{\text{SO}}$  for the other, and is in the topologically trivial  $z$ -AFI if  $|\tilde{\delta}_\alpha| > 3\sqrt{3}\lambda_{\text{SO}}$  for both up and down spins.

In the absence of the alternating sublattice potential,  $\delta = 0$ , there is the additional symmetry  $\Sigma_{A;\alpha}(0) = \Sigma_{B;\bar{\alpha}}(0)$  between the spin-up and the spin-down sublattices of the Néel AF state, where  $\bar{\alpha}$  denotes the opposite direction of  $\alpha$ . This leads to  $\tilde{\delta}_\uparrow = -\tilde{\delta}_\downarrow$  which excludes the possibility of the emergence of the AFI. This originates from the fact that for  $\delta = 0$  the electronic state is invariant under the combination of the time-reversal and the inversion transformations [22–24].

In the  $xy$ -AF state the spin diagonal elements obey the spin symmetry  $\Sigma_{i;\uparrow\uparrow}(0) = \Sigma_{i;\downarrow\downarrow}(0) =: \Sigma_i(0) \in \mathbb{R}$  and the sublattice symmetry  $\Sigma_A(0) = -\Sigma_B(0)$ . For the spin off-diagonal elements one has  $\Sigma_{i;\uparrow\downarrow}(0) = \Sigma_{i;\downarrow\uparrow}^*(0)$  and  $\Sigma_{A;\uparrow\downarrow}(0) = -\Sigma_{B;\uparrow\downarrow}(0)$ . This simplifies the topological Hamiltonian (2) to the Kane-Mele model with the effective spin-independent sublattice potential  $\tilde{\delta} = \delta + \Sigma_A(0)$  subjected to the effective staggered in-plane magnetic field

$$\vec{h}_A = -\vec{h}_B = 2(-\text{Re}[\Sigma_{A;\uparrow\downarrow}(0)], +\text{Im}[\Sigma_{A;\uparrow\downarrow}(0)], 0)^\top \quad , \quad (4)$$

with  $\vec{h}_A$  and  $\vec{h}_B$  acting respectively on the sublattice  $A$  and on the sublattice  $B$ . An infinitesimal staggered in-plane magnetic field (4) makes the edge states gapped and the system becomes

a trivial insulator [66]. Hence, the  $xy$ -AF phase is always topologically trivial.

In the limit of large  $J_K$  the system is in the paramagnetic KI state. The self-energy has no spin off-diagonal element and the diagonal elements are spin-independent. At zero frequency the self-energy is real and obeys the sublattice symmetry  $\Sigma_A(0) = -\Sigma_B(0)$ . The topological Hamiltonian is given by the Kane-Mele model with the effective alternating sublattice potential  $\tilde{\delta} = \delta + \Sigma_A(0)$ . This is just a special case of the above topological Hamiltonians derived in the magnetically ordered phases. We find that the zero-frequency self-energy in the KI phase is always very large such that  $|\tilde{\delta}| > 3\sqrt{3}\lambda_{SO}$  and hence the KI always falls in the topologically trivial region. It should be mentioned that in the KI phase the self-energy at zero frequency diverges (zeroes in the Green's function occur) for  $\delta \rightarrow 0$  which is the responsible mechanism for the gap opening. It is demonstrated by direct evaluation of the Ishikawa-Matsuyama formula that the KI phase at  $\delta = 0$  is topologically trivial [30].

The combination of the DMFT and the topological Hamiltonian method is widely used to map out the phase diagram of different interacting topological models [34–37, 48, 67, 68]. The result obtained for the phase diagram of the Haldane-Hubbard model is in qualitative agreement with the results obtained by other methods such as the ED [36] and the density-matrix renormalization group [69]. A systematic treatment of the non-local quantum fluctuations beyond the DMFT also indicates only minor changes to the phase boundaries [70]. Accordingly, we believe our results to be qualitatively reliable and including the non-local quantum fluctuations to have only minor effects on the phase boundaries.

We emphasize that our characterization of different topological phases does not rely solely on the topological Hamiltonian method. We address the charge excitations in the bulk and at the edges directly for the interacting model (1). We show that there is a finite charge gap in the bulk and at the edges for topologically trivial phases while in the AFCI phase there are gapless charge excitations localized at the edges for only one spin component. Moreover, we show the tendency for the charge gap closing in the KMK model at the location of the topological transition points predicted by the topological Hamiltonian.

### III. PHASE DIAGRAM

In this section we map out the  $T = 0$  phase diagram of the KMK model (1) in the  $J_K$ - $\delta$  plane for the spin-orbit coupling  $\lambda_{SO} = 0.2t$ . To distinguish the different phases we compute three different quantities. The magnitude of the local magnetization of itinerant electrons  $m := |\langle \vec{s}_i \rangle|$  and the localized spins  $M := |\langle \vec{S}_i \rangle|$  pinpoint the transition from the magnetically ordered phase to the paramagnetic KI state. One notes that the lattice always has the Néel AF order and at each lattice site the spin of itinerant electrons  $\langle \vec{s}_i \rangle$  and the localized spin  $\langle \vec{S}_i \rangle$  are antiparallel. We consider Néel AF solutions with the local magnetization not only perpendicular to the honeycomb plane,  $z$ -AF solution, but also parallel to it,  $xy$ -AF solution.

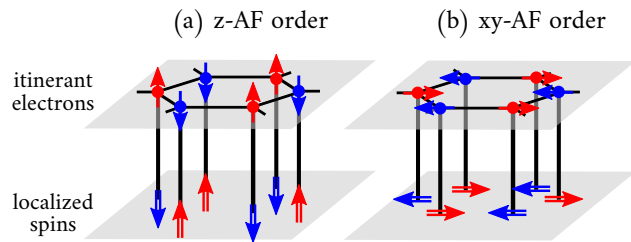


FIG. 2. Schematic representation of the  $z$ -AF order (a) and the  $xy$ -AF order (b) in the Kane-Mele-Kondo model with an AF Kondo interaction between the spin of itinerant electrons and the localized spins. The red filled circles stand for the sites with the higher onsite energy and the blue filled circles stand for the sites with the lower onsite energy. The  $xy$ -AF state is continuously degenerate due to the spontaneous breaking of the U(1) symmetry. The  $z$ -AF state is two-fold degenerate due to the spontaneous breaking of the time-reversal symmetry.

A schematic representation of the  $z$ -AF order and the  $xy$ -AF order is given in Fig. 2. We present data for their energy difference per lattice site,  $\varepsilon_z - \varepsilon_{xy}$ , to determine which solution is the ground state. Finally, the effective alternating sublattice potential (3) reveals the topological nature of the  $z$ -AF state. The  $xy$ -AF phase and the KI phase are always topologically trivial as we discussed in the previous section. We first focus on the case  $\delta = 0$  and then consider the effect of a finite  $\delta$ .

Fig. 3 represents the results for the KMK model at  $\delta = 0$ . In panel (a) we have plotted the local magnetization of the itinerant electrons  $m$  and the localized spins  $M$  vs  $J_K$  in the  $z$ -AF solution and in the  $xy$ -AF solution in the absence of the spin-orbit coupling,  $\lambda_{SO} = 0$ . As one can see the results for the two solutions perfectly match. This is the case also for the energy that we find for the two solutions and is expected because for  $\lambda_{SO} = 0$  the Hamiltonian (1) reduces to the Kondo lattice model which obeys the SU(2) symmetry. This serves as a test for the solutions.

Upon introducing the spin-orbit coupling  $\lambda_{SO} = 0.2t$  in Fig. 3(b) the results for the  $z$ -AF solution and the  $xy$ -AF solution no longer coincide. The  $xy$ -AF solution persists to larger values of the Kondo interaction while the  $z$ -AF solution closes at a smaller value of  $J_K$  in contrast to the results in Fig. 3(a). The data are for the number of bath sites  $n_b = 5$  except for the filled gray squares at  $J_K = 1.7t$  which are for  $n_b = 7$  for the  $z$ -AF solution corroborating the accuracy of the results. The energy difference per lattice site between the  $z$ -AF solution and the  $xy$ -AF solution,  $\varepsilon_z - \varepsilon_{xy}$ , depicted in Fig. 3(c) reveals that the  $xy$ -AF solution always has the lower energy. The results given for the different number of bath sites  $n_b = 5$  and 6 indicate the accuracy of the data. There is only a small difference between the data for  $n_b = 5$  and 6 near the peak of the graph at  $J_K \approx 1.4t$  otherwise they perfectly match. One notes that for  $J_K > 1.85t$  the  $z$ -AF solution in Fig. 3(b) undergoes a transition to the KI and accordingly Fig. 3(c) for  $J_K > 1.85t$  exhibits the energy difference between the KI state and the  $xy$ -AF state. The results in Figs. 3(b) and 3(c) unveil that the KMK model at  $\delta = 0$  displays only a single

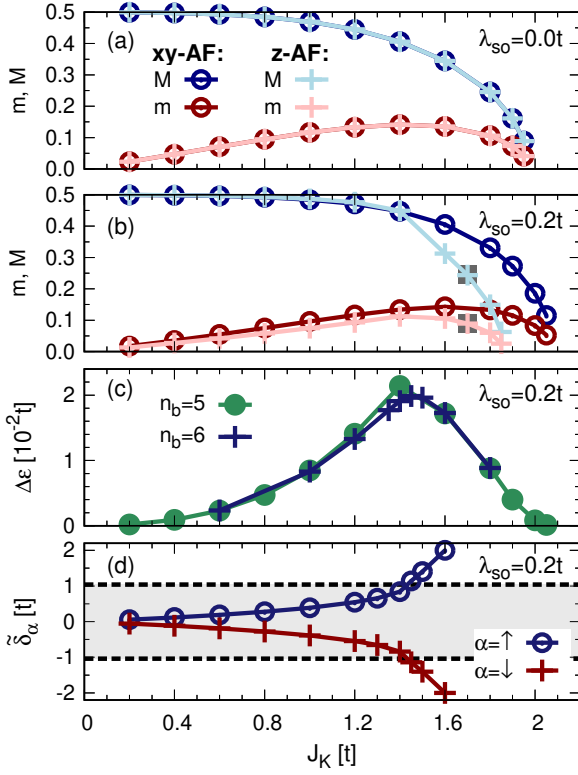


FIG. 3. The results for Kane-Mele-Kondo model (1) at the alternating sublattice potential  $\delta = 0$ . (a),(b) The magnitude of the local magnetization of the itinerant electrons  $m$  and the localized spins  $M$  in the  $z$ -AF solution and in the  $xy$ -AF solution vs the Kondo interaction  $J_K$  for the spin-orbit coupling  $\lambda_{SO} = 0$  in (a) and  $\lambda_{SO} = 0.2t$  in (b). (c) The energy difference per lattice site between the  $z$ -AF solution and the  $xy$ -AF solution,  $\Delta\epsilon = \epsilon_z - \epsilon_{xy}$ , vs  $J_K$  for  $\lambda_{SO} = 0.2t$ . For  $J_K > 1.85t$  the  $z$ -AF solution in panel (b) undergoes a transition to the KI and accordingly panel (c) for  $J_K > 1.85t$  exhibits the energy difference between the KI state and the  $xy$ -AF state. (d) The effective alternating sublattice potential (3) vs  $J_K$  for  $\lambda_{SO} = 0.2t$ . The dashed lines separate the topological region (solid area) from the trivial region. The results in panels (a), (b), and (d) are for the number of bath sites  $n_b = 5$  in the ED impurity solver except for the filled gray squares in panel (b) at  $J_K = 1.7t$  which are for  $n_b = 7$  in the  $z$ -AF solution.

phase transition from the topologically trivial  $xy$ -AFI to the topologically trivial KI upon increasing  $J_K$ . No non-trivial topological phase stabilizes. We would like to mention that we have produced not one, but multiple  $xy$ -AF solutions for some selective points checking that they all display the same magnitude of the local magnetization and the same energy as is expected from the spontaneous breaking of the  $U(1)$  symmetry.

The half-filled KMK model (1) at  $\delta = 0$  is investigated in a number of previous studies focusing on the paramagnetic solutions only [28] but including also the AF solutions [29, 30]. The AF solutions, however, are still restricted to only the  $z$ -AF ordering. The possibility for the  $xy$ -AF ordering is not taken into account. Two quantum phase transitions are identified upon increasing the Kondo interaction  $J_K$ . The first is

from the AFQSHI to the trivial AFI and the second is from the trivial AFI to the KI. Our results for the local magnetization in Fig. 3(b) and the effective alternating sublattice potential (3) plotted in Fig. 3(d) indeed confirms this picture for the  $z$ -AF solution. The dashed lines at  $|\tilde{\delta}_\alpha| = 3\sqrt{3}\lambda_{SO}$  in Fig. 3(d) separate the topological region (solid area) from the trivial region. The transition from the  $z$ -AFQSHI to the trivial  $z$ -AFI occurs at  $J_K \approx 1.4t$  where  $\tilde{\delta}_\uparrow = -\tilde{\delta}_\downarrow$  crosses the dashed line. The transition point found at the smaller value  $J_K \approx 0.7t$  in Ref. 30 is due to the smaller spin-orbit coupling  $\lambda_{SO} = 0.1t$  used, which is half the value  $\lambda_{SO} = 0.2t$  used in our calculations. It should also be noted that in Ref. 30 the numerical renormalization group is employed as the impurity solver while our analysis relies on the ED solver. Hence, while our results for the  $z$ -AF solution agree with the previous studies we find that the stable phase is the topologically trivial  $xy$ -AFI which undergoes a direct transition to the KI upon increasing  $J_K$ .

In addition to hosting the AFQSHI the  $z$ -AF order is intriguing because it exhibits the restoration of topological properties at finite temperatures [30]. Even the topologically trivial  $z$ -AFI manifests non-trivial topological properties as the temperature is raised. Although our findings exclude the possibility of the  $z$ -AF ordering at  $\delta = 0$  one might ask if such a phase can still be realized under some circumstances. In the following we uncover that introducing the alternating sublattice potential  $\delta$  can stabilize the  $z$ -AF order, and show that not only the AFQSHI but also the APCI phase emerge.

Fig. 4 displays the results for the KMK model (1) at  $\delta = 0.8t$  and the spin-orbit coupling  $\lambda_{SO} = 0.2t$ . For these parameters  $\delta < 3\sqrt{3}\lambda_{SO}$  and the Kane-Mele model lies in the QSHI region. The results for the local magnetization of the itinerant electrons  $m$  and the localized spins  $M$  in the  $z$ -AF solution and in the  $xy$ -AF solution plotted in Fig. 4(a) vs the Kondo interaction indicate that the  $xy$ -AF phase still persists up to larger values of  $J_K$  in contrast to the  $z$ -AF phase. We find no  $z$ -AF solution for  $J_K > 1.95t$ . The energy difference between the  $z$ -AF solution and the  $xy$ -AF solution per lattice site  $\Delta\epsilon = \epsilon_z - \epsilon_{xy}$  in Fig. 4(b) reveals that for small  $J_K$  it is the  $z$ -AF solution which has the lower energy. As  $J_K$  is increased the energy difference  $\Delta\epsilon$  crosses the zero-energy line (denoted as a black dashed line) at  $J_K \approx 1.6t$  and a spin-flop transition to the  $xy$ -AF phase takes place. One notes that for  $J_K > 1.95t$  the  $z$ -AF solution no longer exists and Fig. 4(b) compares instead the energy of the KI solution and the  $xy$ -AF solution,  $\Delta\epsilon = \epsilon_{KI} - \epsilon_{xy}$ . The data given for the two different numbers of bath sites  $n_b = 5$  and  $6$  in Fig. 4(b) confirm the accuracy of the results.

To determine the topological nature of the  $z$ -AF phase the effective alternating sublattice potential (3) is plotted vs  $J_K$  in Fig. 4(c). The black dashed lines separate the topological region  $|\tilde{\delta}_\alpha| < 3\sqrt{3}\lambda_{SO}$  from the trivial region  $|\tilde{\delta}_\alpha| > 3\sqrt{3}\lambda_{SO}$ . For small values of  $J_K$  both  $\uparrow$  and  $\downarrow$  spins fall in the topological region, specified by the solid area, and the system is a  $z$ -AFQSHI characterized by the spin Chern number  $\mathcal{C}_s = (\mathcal{C}_\uparrow - \mathcal{C}_\downarrow)/2 = 1$ . Upon increasing  $J_K$  one spin (spin  $\downarrow$  in the figure) leaves the topological region at  $J_K \approx 0.8t$  while the other remains topological. This leads to a non-zero total Chern number  $\mathcal{C} = \mathcal{C}_\uparrow + \mathcal{C}_\downarrow$  and the stabilization of a  $z$ -AFCI.

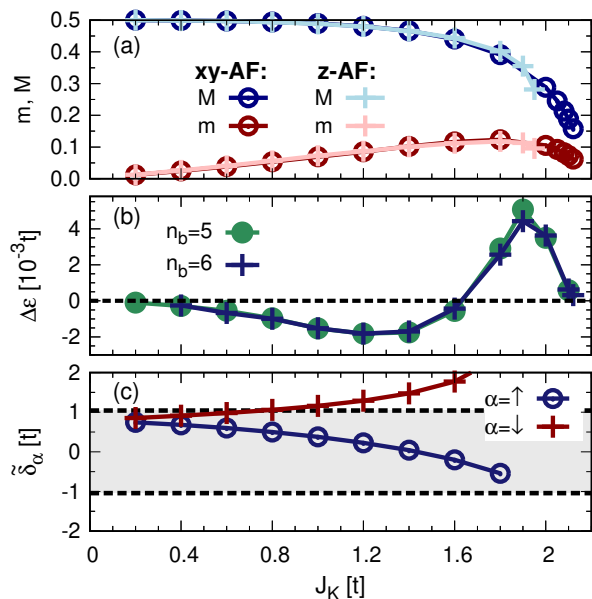


FIG. 4. The results for the Kane-Mele-Kondo model (1) with the alternating sublattice potential  $\delta = 0.8t$  and the spin-orbit coupling  $\lambda_{SO} = 0.2t$ . (a) The magnitude of the local magnetization of the itinerant electrons  $m$  and the localized spins  $M$  in the  $z$ -AF solution and in the  $xy$ -AF solution vs the Kondo interaction  $J_K$ . (b) The energy difference per lattice site between the  $z$ -AF solution and the  $xy$ -AF solution,  $\Delta\varepsilon = \varepsilon_z - \varepsilon_{xy}$ , vs  $J_K$ . For  $J_K > 1.95t$  the  $z$ -AF solution does not exist and panel (b) compares the energy difference between the Kondo insulator (KI) solution and the  $xy$ -AF solution instead. (c) The effective alternating sublattice potential (3) vs  $J_K$ . The dashed lines separate the topological region (solid area) from the trivial region. The results in panels (a) and (c) are for the number of bath sites  $n_b = 5$  in the ED impurity solver.

One notes that a  $z$ -AF state is two-fold degenerate due to the spontaneous breaking of the time-reversal symmetry. The results given in Fig. 4(c) correspond to the  $z$ -AF solution with the local magnetization of the itinerant electrons  $\langle s_i^z \rangle$  positive on the higher-energy sublattice  $A$  and negative on the lower-energy sublattice  $B$ .

Overall, the results in Fig. 4 support three consecutive phase transitions upon increasing  $J_K$ . The first is from the  $z$ -AFQSHI to the  $z$ -AFCI at  $J_K \approx 0.8t$  revealed in Fig. 4(c). The  $z$ -AFCI persists up to  $J_K \approx 1.6t$  where the spin-flop transition to the  $xy$ -AFI in Fig. 4(b) occurs. The  $xy$ -AFI undergoes the third phase transition to the KI at  $J_K \approx 2.15t$  as can be seen from Fig. 4(a).

The energy difference between the  $z$ -AF phase and the  $xy$ -AF phase per lattice site for  $\delta = 0.8t$  in Fig. 4(b) indicates a rather complex behavior in contrast to the results for  $\delta = 0$  in Fig. 3(c). For  $\delta = 0$  the  $xy$ -AF phase always has the lower energy while for the finite value of the alternating sublattice potential  $\delta = 0.8t$  it is the  $z$ -AF phase which becomes the ground state if  $J_K$  is not too large. To see more apparently how the alternating sublattice potential  $\delta$  renders the stabilization of the  $z$ -AF phase we have plotted in Fig. 5 the energy difference  $\varepsilon_z - \varepsilon_{xy}$  vs  $\delta$  for various values of the Kondo in-

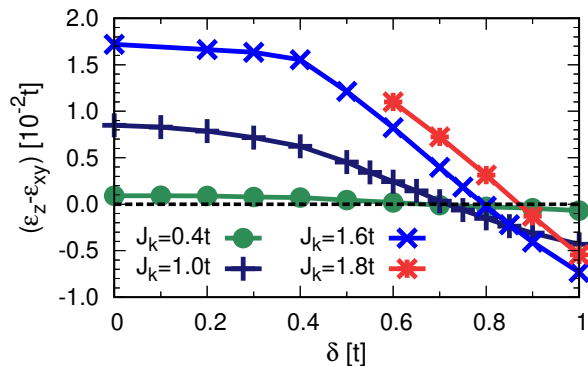


FIG. 5. The energy difference per lattice site between the  $z$ -AF state and the  $xy$ -AF state vs the alternating sublattice potential  $\delta$  for various values of the Kondo interaction  $J_K$ . The spin-orbit coupling is fixed to  $\lambda_{SO} = 0.2t$  and the number of bath sites in the ED impurity solver is given by  $n_b = 5$ .

teraction  $J_K$ . The spin-orbit coupling  $\lambda_{SO} = 0.2t$  and the number of bath sites  $n_b = 5$ . One can see that for small values of  $\delta$  the  $xy$ -AF phase is always the stable solution. However, upon increasing  $\delta$  a spin-flop transition to the  $z$ -AF phase takes place. For the Kondo interaction  $J_K \lesssim 1.0t$  the spin-flop transition almost always occurs at the constant value  $\delta \approx 0.7t$ . As the Kondo interaction is increased beyond  $J_K \approx 1.0t$  the position of the spin-flop transition starts shifting to larger values of  $\delta$ . The spin-flop transition found at  $J_K \approx 1.6t$  in Fig. 4(b) for  $\delta = 0.8t$  upon varying  $J_K$  is nicely in agreement with the spin-flop transition obtained at  $\delta \approx 0.8t$  in Fig. 5 for  $J_K = 1.6t$  upon varying  $\delta$ .

We proceed to the rather large value of the alternating sublattice potential  $\delta = 2t$ . For this value of  $\delta$  the Kane-Mele model falls into the trivial insulator phase. Whence, a topologically trivial AF insulator is expected for weak Kondo interactions. In Fig. 6 we have plotted the same quantities as in Fig. 4 but for the alternating sublattice potential  $\delta = 2t$ . In contrast to Figs. 3(b) and 4(a) it is the  $z$ -AF solution in Fig. 6(a) which persists to larger values of the Kondo interaction  $J_K$ . We find a discontinuous transition from the  $z$ -AF phase to the KI at  $J_K \approx 3.05t$ . Fig. 6(b) compares the energy of the  $z$ -AF solution and the  $xy$ -AF solution,  $\Delta\varepsilon = \varepsilon_z - \varepsilon_{xy}$ , for  $J_K \leq 1.9t$  and the energy of the  $z$ -AF solution and the paramagnetic KI solution,  $\Delta\varepsilon = \varepsilon_z - \varepsilon_{KI}$ , for  $J_K \geq 2.6t$ . The  $xy$ -AF solution exists up to  $J_K \approx 1.9t$  and the KI solution exists down to  $J_K \approx 2.6t$ . For  $1.9t < J_K < 2.6t$  the  $z$ -AF solution is the only solution, which is why there is no data in this parameter range in Fig. 6(b). The results in Fig. 6(b) reveal that for  $\delta = 2t$  the  $z$ -AF solution is always the stable phase in the coexistence regions.

The effective alternating sublattice potential (3) plotted in Fig. 6(c) unveils a transition from the topologically trivial  $z$ -AFI to the  $z$ -AFCI at  $J_K \approx 2t$ , which corresponds to the spin  $\uparrow$  entering the topological region (solid area). Similar to the results in Fig. 4(c) the results in Fig. 6(c) are for the  $z$ -AF solution with the local magnetization of the itinerant electrons  $\langle s_i^z \rangle$  positive on the higher-energy sublattice  $A$  and negative

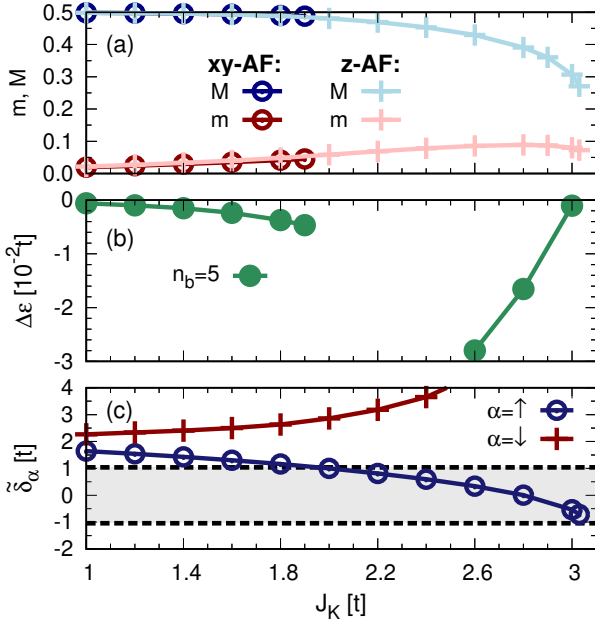


FIG. 6. The results for the Kane-Mele-Kondo model (1) with the alternating sublattice potential  $\delta = 2t$  and the spin-orbit coupling  $\lambda_{SO} = 0.2t$ . (a) The magnitude of the local magnetization of the itinerant electrons  $m$  and the localized spins  $M$  in the  $z$ -AF solution and in the  $xy$ -AF solution vs the Kondo interaction  $J_K$ . (b) The energy difference between the  $z$ -AF solution and the  $xy$ -AF solution,  $\Delta\epsilon = \epsilon_z - \epsilon_{xy}$ , for  $J_K \leq 1.9t$  and between the  $z$ -AF solution and the Kondo insulator solution for  $J_K \geq 2.6t$ . For  $1.9t < J_K < 2.6t$  the  $z$ -AF solution is the only solution which is why there is no data in this parameter range in panel (b). (c) The effective alternating sublattice potential (3) vs  $J_K$ . The dashed lines separate the topological region (solid area) from the trivial region. The results are for the number of bath sites  $n_b = 5$  in the ED impurity solver.

on the lower-energy sublattice  $B$ . Applying the time-reversal transformation one can access the other solution, for which it is the spin  $\downarrow$  that enters the topological region. The system stays in the  $z$ -AFCI up to  $J_K \approx 3.05t$  where the transition to the KI takes place, see Fig. 6(a). We have produced data also for larger values of  $\delta$  and found similar phase transitions except that occurring at larger values of  $J_K$ .

The phase diagram in Fig. 7 concludes our findings in this section. The results are for the spin-orbit coupling  $\lambda_{SO} = 0.2t$ . The number of bath sites used in the ED impurity solver is  $n_b = 5$  although increasing the number of bath sites is not expected to change the phase boundaries. For small values of the alternating sublattice potential  $\delta$  the system is in the topologically trivial  $xy$ -AFI which undergoes a transition to the topologically trivial KI upon increasing the Kondo interaction. For large values of  $\delta$  the topologically trivial  $z$ -AFI at the weak Kondo coupling and the KI at the strong Kondo coupling are separated by an intermediate  $z$ -AFCI. The  $z$ -AFCI appears around  $\delta = 3J_K/4$ . The  $z$ -AFQSHI is stabilized at moderate values of  $\delta$  and the weak Kondo interaction. The phase diagram in Fig. 7 modifies and generalizes the previous phase diagrams [28–30] proposed for the half-filled KMK

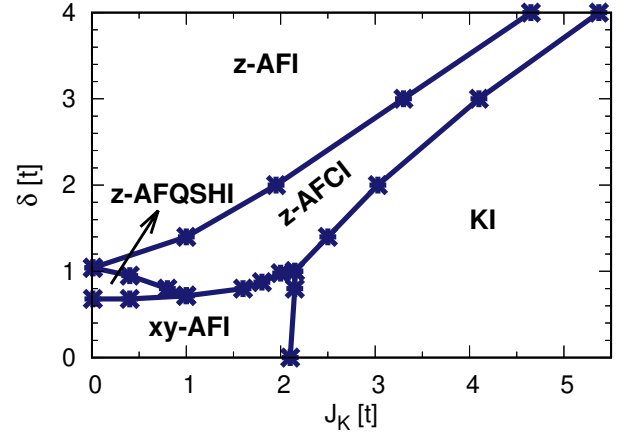


FIG. 7. The phase diagram of the KMK model (1) for the spin-orbit coupling  $\lambda_{SO} = 0.2t$ . The topologically trivial phases are the  $z$ -AF insulator ( $z$ -AFI), the  $xy$ -AF insulator ( $xy$ -AFI), and the Kondo insulator (KI). The non-trivial topological phases are the  $z$ -AF Chern insulator ( $z$ -AFCI) and the  $z$ -AF quantum spin Hall insulator ( $z$ -AFQSHI). The results are for the number of bath site  $n_b = 5$  in the ED impurity solver.

model at zero temperature.

A clarification on the existence of the  $z$ -AFQSHI at a finite  $\delta$  in Fig. 7 is in order. The time-reversal symmetry is often considered necessary for the realization of the QSHI protecting the state against spin-mixing terms such as the Rashba spin-orbit coupling [31, 71]. For the AFQSHI the combination of the time-reversal transformation and a lattice translation is considered to play the role of the protecting symmetry [72, 73]. The QSHI, however, is found to remain immune against the Rashba spin-orbit coupling even in the presence of a perpendicular Zeeman field perturbation breaking the time-reversal symmetry [74–77]. The  $z$ -AFQSHI appearing at a finite  $\delta$  in Fig. 7 is also expected to be robust against the spin-mixing terms despite the absence of a lattice translation to compensate the effect of the time-reversal transformation [33]. There is usually a sub-symmetry in the system protecting the edge states [78] although finding it is not always trivial [77]. An explicit analysis of the effect of the Rashba spin-orbit coupling on the edge states in the  $z$ -AFQSHI and the existence of a certain hidden symmetry deserve future attention.

The stabilization of the  $z$ -AFQSHI and the  $z$ -AFCI in Fig. 7 is a consequence of the combined effect of the spin-orbit coupling, the electronic correlation, and the alternating sublattice potential. The  $z$ -AFCI is reported also in some other models of strongly correlated systems under similar conditions but for transition-metal compounds [22–25]. The Mott insulator phase in the strongly interacting regime of these models is always magnetically ordered in contrast to the paramagnetic KI phase in Fig. 7 which is the characteristic of heavy-fermion systems.

#### IV. CHARGE EXCITATIONS

This section is devoted to a comprehensive study of charge excitations in the KMK model with a three-fold aim. First, we confirm that for the topologically trivial phases in Fig. 7 the charge excitations are gapped in the bulk and at the edges but for the  $z$ -AFCI there are gapless excitations localized at the edges for only one spin component. This demonstrates the topological nature of these phases beyond the topological Hamiltonian method. Second, we examine that the topological phase transition from the trivial  $z$ -AFI to the  $z$ -AFCI predicted based on the topological Hamiltonian is accompanied by closing of the bulk charge gap in the KMK model. Finally, we address the dependence of the charge gap on the spin-orbit coupling in the  $z$ -AFCI. This allows a systematic comparison between the size of the charge gap in the AFCI in heavy-fermion systems and the size of the charge gap in the AFCI reported for transition-metal compounds [25].

To investigate the charge excitations in the bulk and at the edges we consider a cylindrical geometry of the size  $L \times L$  with  $L = 40$ . We consider the periodic boundary condition in  $y$  and the open boundary condition in  $x$  direction with the edges at  $x = 0$  and  $x = 39$ . We compute the single-particle spectral function

$$\begin{aligned} A_x(\omega) &:= \frac{1}{2} \sum_{\alpha=\uparrow,\downarrow} A_{x,\alpha}(\omega) \\ &:= \frac{1}{4} \sum_{\alpha=\uparrow,\downarrow} (A_{x,y;\alpha}(\omega) + A_{x,y+1;\alpha}(\omega)) \end{aligned} \quad (5)$$

where  $A_{x,y;\alpha}(\omega)$  is the local spectral function at the lattice position  $(x, y)$  for spin  $\alpha$ . The Lorentzian broadening with a broadening factor of  $0.05t$  is used in the calculations. In Eq. (5) we have averaged over the spin and the two non-equivalent lattice sites in the  $y$  direction. The spin-resolved spectral function  $A_{x,\alpha}(\omega)$  is utilized in the case we aim to distinguish the contributions of different spins to the spectral function.

The spectral function (5) is plotted in Fig. 8 around the Fermi energy  $\omega = 0$  for  $\lambda_{\text{SO}} = 0.2t$  and different values of the alternating sublattice potential  $\delta$  and the Kondo interaction  $J_K$  corresponding to the different phases  $z$ -AFI,  $z$ -AFCI, KI, and  $xy$ -AFI. We find the spectral function  $A_x(\omega)$  perfectly symmetric with respect to the center of the cylinder which is why we have included only the results for  $x < 20$  in Fig. 8. The spectral function  $A_x(\omega)$  becomes independent of  $x$  as we move away from the edges. This can be seen in all the panels in Fig. 8 as the results for  $x = 8$  nicely agree with the results for  $x = 19$ , matching perfectly also with the spectral function that we obtain by applying periodic boundary conditions in both directions.

As one can see from Figs. 8(a), (c), and (d) the charge excitations in the topologically trivial phases are gapped in the bulk and at the edges. In contrast, there is a finite spectral weight at the Fermi energy  $\omega = 0$  in the  $z$ -AFCI in Fig. 8(b) for  $x = 0$  which quickly disappears as the bulk is approached. The spin-resolved spectral function  $A_{x=0,\alpha}(\omega)$  depicted in the inset of Fig. 8(b) verifies that the gapless excitations is

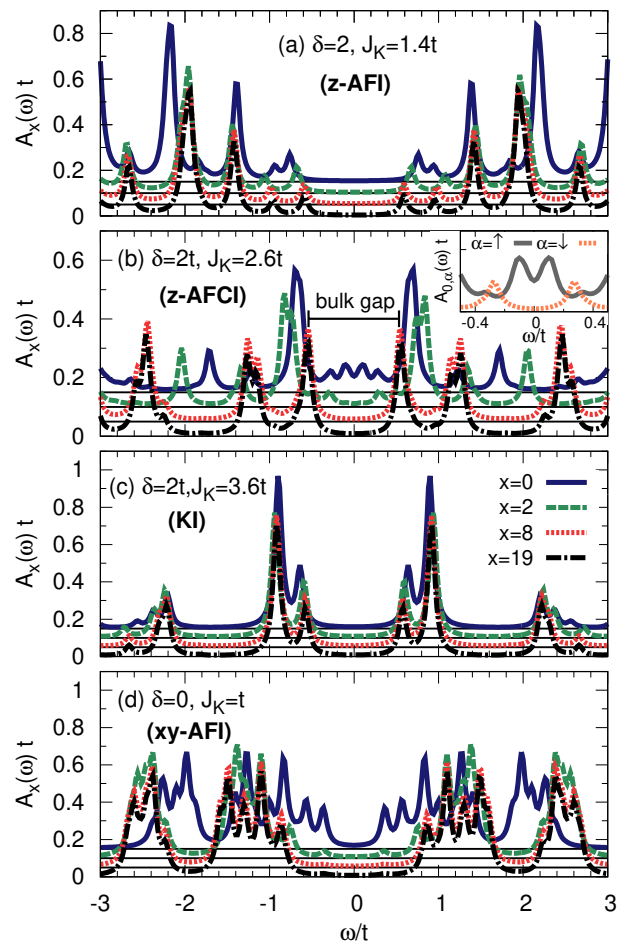


FIG. 8. Single-particle spectral function (5) plotted vs frequency  $\omega$  around the Fermi energy  $\omega = 0$  at various values of  $x$  for a cylindrical geometry of size  $40 \times 40$  with periodic boundary conditions in  $y$  and open boundary conditions in  $x$  direction. The edges are at  $x = 0$  and  $x = 39$ . The spin-orbit coupling  $\lambda_{\text{SO}} = 0.2t$  and the number of bath sites in the ED impurity solver  $n_b = 5$ . The different panels represent results for different values of the alternating sublattice potential  $\delta$  and the Kondo interaction  $J_K$ , which are chosen to correspond to the different phases in the phase diagram in Fig. 7. The horizontal bar in the panel (b) denotes the bulk gap and the inset exhibits the edge spin-resolved spectral function  $A_{x=0,\alpha}(\omega)$ .

due to the spin  $\uparrow$  which is the one entering the topological region in Fig. 6(c). This demonstrates the existence of the  $z$ -AFCI directly for the interacting model (1) going beyond the topological Hamiltonian method.

The topological phase transition from the trivial  $z$ -AFI to the  $z$ -AFCI predicted by the topological Hamiltonian upon increasing the Kondo interaction  $J_K$  in Fig. 6(c) has to be accompanied by the softening of the charge gap in the KMK model (1). This is necessary for the Chern number to change across the phase transition. In Fig. 9 we have plotted the charge gap  $\Delta_\alpha$  for spin  $\alpha$  vs the Kondo interaction  $J_K$  for the alternating sublattice potential  $\delta = 2t$ . The spin-orbit coupling is set to  $\lambda_{\text{SO}} = 0.2t$ . The charge gap  $\Delta_\alpha$  is extracted



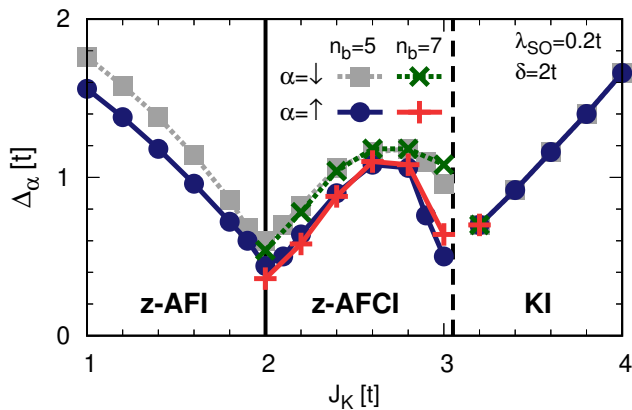


FIG. 9. Spin-resolved charge gap vs the Kondo interaction  $J_K$  for the alternating sublattice potential  $\delta = 2t$  and the spin-orbit coupling  $\lambda_{SO} = 0.2t$ . The vertical solid line denotes the position of the transition point from the topologically trivial  $z$ -AF insulator ( $z$ -AFI) to the  $z$ -AF Chern insulator ( $z$ -AFCI) predicted by the topological Hamiltonian. The vertical dashed line depicts the position of the first-order transition point from the  $z$ -AFCI to the Kondo insulator (KI). In the intermediate region the results for the number of bath sites  $n_b = 5$  and  $7$  are compared.

from the spin-resolved spectral functions obtained using periodic boundary conditions in both directions for a lattice of size  $L \times L$  with  $L = 40$ . The charge gap is given by the distance between the electron and the hole peaks closest to the Fermi energy  $\omega = 0$  in the spectral function. This is illustrated by a horizontal bar in Fig. 8(b). The results in Fig. 9 are for the number of bath sites  $n_b = 5$  although in the intermediate region we have provided data also for  $n_b = 7$ . We have produced data also for  $n_b = 6$  in the whole parameter range showing a nice agreement with the results for  $n_b = 5$  and not included in Fig. 9 in order to avoid a busy figure. As in the previous cases the results are for the  $z$ -AF solution with the local magnetization of the itinerant electrons  $\langle s_z^i \rangle$  positive on the higher-energy sublattice  $A$  and negative on the lower-energy sublattice  $B$ , which is why the charge gap for spin  $\uparrow$  is smaller than the charge gap for spin  $\downarrow$  in Fig. 9. The vertical solid line in Fig. 9 specifies the position of the transition point from the trivial  $z$ -AFI to the  $z$ -AFCI predicted by the topological Hamiltonian. The vertical dashed line shows the location of the first-order transition from the  $z$ -AFCI to the KI.

The charge gap in the  $z$ -AFI in Fig. 9 decreases upon increasing the Kondo interaction up to  $J_K = 2t$  and starts increasing as the system enters the  $z$ -AFCI phase. We attribute the finite value of the charge gap at  $J_K = 2t$  to the finite number of bath sites in the impurity solver. One can see a tendency towards a smaller charge gap at  $J_K = 2t$  upon increasing the number of bath sites. Capturing a truly vanishing gap at the transition point would require an infinite number of bath sites, i.e., a continuous representation of the bath. We conclude that the minimum of the charge gap occurring at  $J_K = 2t$  is nicely in agreement with the prediction of the topological Hamiltonian for a transition from the  $z$ -AFI to the  $z$ -AFCI. As the effective alternating sublattice potential for spin  $\uparrow$  in Fig. 6(c)

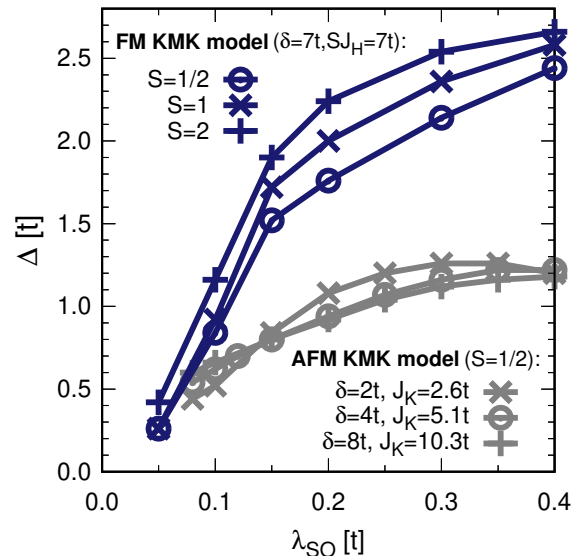


FIG. 10. Charge gap for the Kane-Mele-Kondo (KMK) model vs the spin-orbit coupling  $\lambda_{SO}$  in the  $z$ -AF Chern insulator ( $z$ -AFCI) phase. The size of the localized spin is denoted by  $S$  and the alternating sublattice potential by  $\delta$ . The figure involves the data for both the antiferromagnetic Kondo interaction (AFM KMK model) controlled by  $J_K$  and the ferromagnetic Kondo interaction (FM KMK model) controlled by  $SJ_H$ . The results are for the number of bath sites  $n_b = 5$  in the ED impurity solver. The data for the FM KMK model are from Ref. 25.

approaches the lower boundary of the topological region at  $\delta_\alpha \approx -1.04t$  we observe also a decrease in the charge gap in Fig. 9 until the first-order transition to the KI happens. In the KI phase the charge gap becomes spin-independent and increases upon increasing the Kondo interaction as is expected.

The  $z$ -AFCI is found in various single-orbital [22–24] and multi-orbital [25] models of transition-metal compounds. The multi-orbital analysis relies on the KMK model with a *ferromagnetic* Kondo interaction (Hund coupling  $J_H > 0$ ) between the electron spins and the localized spins. Different sizes of the localized spin  $S = 1/2, 1, 2$  corresponding to different numbers of orbitals are addressed [25]. In Fig. 10 we have plotted the charge gap vs the spin-orbit coupling in the  $z$ -AFCI phase. The figure involves not only the data for the KMK model with the AF Kondo interaction (AFM KMK model) controlled by  $J_K$  but also the data for the KMK model with the ferromagnetic Kondo interaction (FM KMK model) controlled by  $SJ_H$ . The data for the FM KMK model are from Ref. 25. The results in Fig. 10 allows a systematic comparison between the size of the charge gap in the  $z$ -AFCI in heavy-fermion materials and in transition-metal compounds.

The values for the alternating sublattice potential and the Kondo interaction in Fig. 10 are chosen such that the system falls in the AFCI phase. We see only negligible changes in the charge gap in the AFM KMK model despite the significant change in the alternating sublattice potential  $\delta$ . This shows that the results do not depend on the details of the model and represent the generic behavior of the charge gap in the AFCI

in heavy-fermion systems. No significant change in the charge gap is observed also in the FM KMK model for various sizes of the localized spin and hence the results for the FM KMK model are also expected to manifest the generic behavior of the charge gap in transition-metal compounds. The results in Fig. 10 unveil the fact that the AFCI exists in transition-metal compounds with a larger charge gap than in heavy-fermion systems. This suggests that it is not solely the spin-orbit coupling which determines the size of the charge gap in an AFCI and other mechanisms are also involved. The exchange and the double exchange interactions are the responsible mechanisms for the magnetic blueshift of the charge gap observed in multiple theoretical and experimental studies of AF Mott insulators [53, 54, 79]. A future research addressing the mechanisms which govern the charge gap in an AFCI can further pave the path to a higher temperature realization of this intriguing topological state of matter.

## V. CONCLUSION

Heavy-fermion materials display a variety of phases such as metals, unconventional superconductors, trivial and topological Kondo insulators, and different kinds of long-range magnetic orderings. In this paper we explore the possibility for the realization of the AFCI and the AFQSHI in heavy-fermion systems. Our analysis is based on the half-filled KMK model that serves as a paradigm for the study of the effect of the spin-orbit coupling in heavy-fermion systems. We go beyond the previous analyses of the model by considering the Néel AF solutions with the local magnetization oriented not only perpendicular,  $z$ -AF solution, but also parallel,  $xy$ -AF solution, to the honeycomb plane. Comparing the energies of the two solutions reveals that in the absence of the alternating sublattice potential it is the  $xy$ -AF solution which is always the stable phase. The model undergoes a transition from the  $xy$ -AFI to the KI upon increasing the Kondo interaction  $J_K$ . No non-trivial topological phase occurs. Our results modify the previ-

ous findings for the phase diagram of the model restricted only to the paramagnetic and the  $z$ -AF solutions [28–30]. We address the effect of a finite alternating sublattice potential  $\delta$  on the system and map out the phase diagram of the KMK model (1) in the plane of  $\delta$  vs  $J_K$ . It is shown that the  $z$ -AF solution can become the stable phase at a finite alternating sublattice potential giving rise to the emergence of the  $z$ -AFCI and the  $z$ -AFQSHI. Two-dimensional materials with strong spin-orbit coupling and buckled structure such as silicene, germanene, and stanene (known as 2D-Xenes) [40] grown on an appropriate magnetic insulating substrate [41] are potential candidates to realize the KMK model with a tunable alternating sublattice potential and the observation of our predicted AF topological insulators.

We perform a comprehensive study of the charge excitations in the system. For the topologically trivial phases the charge excitations are confirmed to be gapped in the bulk and at the edges. In contrast, gapless excitations localized at the edges for only one spin component appear in the spectrum in the  $z$ -AFCI phase. The results for the bulk charge gap across the topological phase transitions exhibit a clear tendency towards a vanishing charge gap at the location of the topological transition points, confirming further the findings based on the topological invariant calculations. A systematic comparison between the size of the charge gap in the AFCI in heavy-fermion materials and in transition-metal compounds indicates a larger charge gap for the AFCI in the latter system for the same strength of the spin-orbit coupling. This suggests that there are other mechanisms in addition to the spin-orbit coupling which determine the charge gap in an AFCI and deserve future attention. Another major outlook of our work is to explore the topological properties at finite temperatures and to examine up to which temperature scale the quantization of the Hall conductance and the gapless edge states can survive.

## REFERENCES

- 
- [1] C.-Z. Chang, J. Zhang, X. Feng, J. Shen, Z. Zhang, M. Guo, K. Li, Y. Ou, P. Wei, L.-L. Wang, Z.-Q. Ji, Y. Feng, S. Ji, X. Chen, J. Jia, X. Dai, Z. Fang, S.-C. Zhang, K. He, Y. Wang, L. Lu, X.-C. Ma, and Q.-K. Xue, Experimental Observation of the Quantum Anomalous Hall Effect in a Magnetic Topological Insulator, *Science* **340**, 167 (2013).
  - [2] Y. Tokura, K. Yasuda, and A. Tsukazaki, Magnetic topological insulators, *Nature Reviews Physics* **1**, 126 (2019).
  - [3] C.-Z. Chang, C.-X. Liu, and A. H. MacDonald, Colloquium: Quantum anomalous Hall effect, *Rev. Mod. Phys.* **95**, 011002 (2023).
  - [4] X. Kou, L. Pan, J. Wang, Y. Fan, E. S. Choi, W.-L. Lee, T. Nie, K. Murata, Q. Shao, S.-C. Zhang, and K. L. Wang, Metal-to-insulator switching in quantum anomalous Hall states, *Nature Communications* **6**, 8474 (2015).
  - [5] M. Mogi, R. Yoshimi, A. Tsukazaki, K. Yasuda, Y. Kozuka, K. S. Takahashi, M. Kawasaki, and Y. Tokura, Magnetic modulation doping in topological insulators toward higher-temperature quantum anomalous Hall effect, *Applied Physics Letters* **107**, 182401 (2015).
  - [6] P. Wang, J. Ge, J. Li, Y. Liu, Y. Xu, and J. Wang, Intrinsic magnetic topological insulators, *The Innovation* **2**, 100098 (2021).
  - [7] Y. Wang, F. Zhang, M. Zeng, H. Sun, Z. Hao, Y. Cai, H. Rong, C. Zhang, C. Liu, X. Ma, L. Wang, S. Guo, J. Lin, Q. Liu, C. Liu, and C. Chen, Intrinsic magnetic topological materials, *Frontiers of Physics* **18**, 21304 (2023).
  - [8] M. M. Otrokov, I. P. Rusinov, M. Blanco-Rey, M. Hoffmann, A. Y. Vyazovskaya, S. V. Ereemeev, A. Ernst, P. M. Echenique, A. Arnau, and E. V. Chulkov, Unique Thickness-Dependent Properties of the van der Waals Interlayer Antiferromagnet MnBi<sub>2</sub>Te<sub>4</sub> Films, *Phys. Rev. Lett.* **122**, 107202 (2019).
  - [9] M. M. Otrokov, I. I. Klimovskikh, H. Bentmann, D. Estyunin, A. Zeugner, Z. S. Aliev, S. Gaß, A. U. B. Wolter, A. V. Koroleva, A. M. Shikin, M. Blanco-Rey, M. Hoffmann, I. P. Rusinov, A. Y. Vyazovskaya, S. V. Ereemeev, Y. M. Koroteev, V. M. Kuznetsov, F. Freyse, J. Sánchez-Barriga, I. R.

- Amiraslanov, M. B. Babanly, N. T. Mamedov, N. A. Abdullayev, V. N. Zverev, A. Alfonsov, V. Kataev, B. Büchner, E. F. Schwier, S. Kumar, A. Kimura, L. Petaccia, G. Di Santo, R. C. Vidal, S. Schatz, K. Kißner, M. Ünzelmann, C. H. Min, S. Moser, T. R. F. Peixoto, F. Reinert, A. Ernst, P. M. Echenique, A. Isaeva, and E. V. Chulkov, Prediction and observation of an antiferromagnetic topological insulator, *Nature* **576**, 416 (2019).
- [10] J. Li, Y. Li, S. Du, Z. Wang, B.-L. Gu, S.-C. Zhang, K. He, W. Duan, and Y. Xu, Intrinsic magnetic topological insulators in van der Waals layered  $\text{MnBi}_2\text{Te}_4$ -family materials, *Science Advances* **5**, eaaw5685 (2019).
- [11] Y. Gong, J. Guo, J. Li, K. Zhu, M. Liao, X. Liu, Q. Zhang, L. Gu, L. Tang, X. Feng, D. Zhang, W. Li, C. Song, L. Wang, P. Yu, X. Chen, Y. Wang, H. Yao, W. Duan, Y. Xu, S.-C. Zhang, X. Ma, Q.-K. Xue, and K. He, Experimental Realization of an Intrinsic Magnetic Topological Insulator, *Chinese Physics Letters* **36**, 076801 (2019).
- [12] H. Li, S.-Y. Gao, S.-F. Duan, Y.-F. Xu, K.-J. Zhu, S.-J. Tian, J.-C. Gao, W.-H. Fan, Z.-C. Rao, J.-R. Huang, J.-J. Li, D.-Y. Yan, Z.-T. Liu, W.-L. Liu, Y.-B. Huang, Y.-L. Li, Y. Liu, G.-B. Zhang, P. Zhang, T. Kondo, S. Shin, H.-C. Lei, Y.-G. Shi, W.-T. Zhang, H.-M. Weng, T. Qian, and H. Ding, Dirac Surface States in Intrinsic Magnetic Topological Insulators  $\text{EuSn}_2\text{As}_2$  and  $\text{MnBi}_{2n}\text{Te}_{3n+1}$ , *Physical Review X* **9**, 041039 (2019).
- [13] Y.-J. Hao, P. Liu, Y. Feng, X.-M. Ma, E. F. Schwier, M. Arita, S. Kumar, C. Hu, R. Lu, M. Zeng, Y. Wang, Z. Hao, H.-Y. Sun, K. Zhang, J. Mei, N. Ni, L. Wu, K. Shimada, C. Chen, Q. Liu, and C. Liu, Gapless Surface Dirac Cone in Antiferromagnetic Topological Insulator  $\text{MnBi}_2\text{Te}_4$ , *Phys. Rev. X* **9**, 041038 (2019).
- [14] Y. J. Chen, L. X. Xu, J. H. Li, Y. W. Li, H. Y. Wang, C. F. Zhang, H. Li, Y. Wu, A. J. Liang, C. Chen, S. W. Jung, C. Cacho, Y. H. Mao, S. Liu, M. X. Wang, Y. F. Guo, Y. Xu, Z. K. Liu, L. X. Yang, and Y. L. Chen, Topological Electronic Structure and Its Temperature Evolution in Antiferromagnetic Topological Insulator  $\text{MnBi}_2\text{Te}_4$ , *Phys. Rev. X* **9**, 041040 (2019).
- [15] Y. Deng, Y. Yu, M. Z. Shi, Z. Guo, Z. Xu, J. Wang, X. H. Chen, and Y. Zhang, Quantum anomalous Hall effect in intrinsic magnetic topological insulator  $\text{MnBi}_2\text{Te}_4$ , *Science* **367**, 895 (2020).
- [16] C. Liu, Y. Wang, H. Li, Y. Wu, Y. Li, J. Li, K. He, Y. Xu, J. Zhang, and Y. Wang, Robust axion insulator and Chern insulator phases in a two-dimensional antiferromagnetic topological insulator, *Nature Materials* **19**, 522 (2020).
- [17] M. Serlin, C. L. Tschirhart, H. Polshyn, Y. Zhang, J. Zhu, K. Watanabe, T. Taniguchi, L. Balents, and A. F. Young, Intrinsic quantized anomalous Hall effect in a moiré heterostructure, *Science* **367**, 900 (2020).
- [18] T. Li, S. Jiang, B. Shen, Y. Zhang, L. Li, Z. Tao, T. Devakul, K. Watanabe, T. Taniguchi, L. Fu, J. Shan, and K. F. Mak, Quantum anomalous Hall effect from intertwined moiré bands, *Nature* **600**, 641 (2021).
- [19] T. Jungwirth, X. Marti, P. Wadley, and J. Wunderlich, Antiferromagnetic spintronics, *Nature Nanotechnology* **11**, 231 (2016).
- [20] V. Baltz, A. Manchon, M. Tsoi, T. Moriyama, T. Ono, and Y. Tserkovnyak, Antiferromagnetic spintronics, *Rev. Mod. Phys.* **90**, 015005 (2018).
- [21] L. Šmejkal, Y. Mokrousov, B. Yan, and A. H. MacDonald, Topological antiferromagnetic spintronics, *Nature Physics* **14**, 242 (2018).
- [22] K. Jiang, S. Zhou, X. Dai, and Z. Wang, Antiferromagnetic Chern Insulators in Noncentrosymmetric Systems, *Phys. Rev. Lett.* **120**, 157205 (2018).
- [23] M. Ebrahimkhas, G. S. Uhrig, W. Hofstetter, and M. Hafez-Torbati, Antiferromagnetic Chern insulator in centrosymmetric systems, *Phys. Rev. B* **106**, 205107 (2022).
- [24] P.-J. Guo, Z.-X. Liu, and Z.-Y. Lu, Quantum anomalous Hall effect in collinear antiferromagnetism, *npj Computational Materials* **9**, 70 (2023).
- [25] M. Hafez-Torbati and G. S. Uhrig, Antiferromagnetic Chern insulator with large charge gap in heavy transition-metal compounds (2024), [arXiv:2402.12918](https://arxiv.org/abs/2402.12918).
- [26] B. Wu, Y.-l. Song, W.-x. Ji, P.-j. Wang, S.-f. Zhang, and C.-w. Zhang, Quantum anomalous Hall effect in an antiferromagnetic monolayer of  $\text{MoO}$ , *Phys. Rev. B* **107**, 214419 (2023).
- [27] A. Georges, G. Kotliar, W. Krauth, and M. J. Rozenberg, Dynamical mean-field theory of strongly correlated fermion systems and the limit of infinite dimensions, *Rev. Mod. Phys.* **68**, 13 (1996).
- [28] X.-Y. Feng, J. Dai, C.-H. Chung, and Q. Si, Competing Topological and Kondo Insulator Phases on a Honeycomb Lattice, *Phys. Rev. Lett.* **111**, 016402 (2013).
- [29] Y. Zhong, Y.-F. Wang, H.-T. Lu, and H.-G. Luo, Topological quantum phase transition in Kane-Mele-Kondo lattice model, *Phys. Rev. B* **88**, 235111 (2013).
- [30] T. Yoshida, R. Peters, and N. Kawakami, Restoration of topological properties at finite temperatures in a heavy-fermion system, *Phys. Rev. B* **93**, 045138 (2016).
- [31] C. L. Kane and E. J. Mele, Quantum spin Hall effect in graphene, *Phys. Rev. Lett.* **95**, 226801 (2005).
- [32] C. L. Kane and E. J. Mele,  $Z_2$  Topological Order and the Quantum Spin Hall Effect, *Phys. Rev. Lett.* **95**, 146802 (2005).
- [33] H. Guo, S. Feng, and S.-Q. Shen, Quantum spin Hall effect induced by nonmagnetic and magnetic staggered potentials, *Phys. Rev. B* **83**, 045114 (2011).
- [34] A. Amaricci, J. C. Budich, M. Capone, B. Trauzettel, and G. Sangiovanni, First-Order Character and Observable Signatures of Topological Quantum Phase Transitions, *Phys. Rev. Lett.* **114**, 185701 (2015).
- [35] M. Hafez-Torbati, J.-H. Zheng, B. Irsigler, and W. Hofstetter, Interaction-driven topological phase transitions in fermionic  $\text{SU}(3)$  systems, *Phys. Rev. B* **101**, 245159 (2020).
- [36] T. I. Vanhala, T. Siro, L. Liang, M. Troyer, A. Harju, and P. Törmä, Topological Phase Transitions in the Repulsively Interacting Haldane-Hubbard Model, *Phys. Rev. Lett.* **116**, 225305 (2016).
- [37] M. Ebrahimkhas, M. Hafez-Torbati, and W. Hofstetter, Lattice symmetry and emergence of antiferromagnetic quantum Hall states, *Phys. Rev. B* **103**, 155108 (2021).
- [38] M. Ezawa, A topological insulator and helical zero mode in silicene under an inhomogeneous electric field, *New Journal of Physics* **14**, 033003 (2012).
- [39] D. Xiao, W. Zhu, Y. Ran, N. Nagaosa, and S. Okamoto, Interface engineering of quantum Hall effects in digital transition metal oxide heterostructures, *Nature Communications* **2**, 596 (2011).
- [40] A. Molle, J. Goldberger, M. Houssa, Y. Xu, S.-C. Zhang, and D. Akinwande, Buckled two-dimensional Xene sheets, *Nature Materials* **16**, 163 (2017).
- [41] A. M. Tokmachev, D. V. Averyanov, I. S. Sokolov, A. N. Taldenkov, O. E. Parfenov, I. A. Karateev, and V. G. Storchak, 14 - Two-dimensional magnetism in Xenex, in *Xenex*, edited by A. Molle and C. Grazianetti (Woodhead Publishing, 2022) pp. 353–375.
- [42] J. H. Van Vleck, *The Theory of Electric and Magnetic Susceptibilities* (Oxford University Press, 1932).
- [43] N. Bloembergen and T. J. Rowland, Nuclear Spin Exchange in Solids:  $\text{Tl}^{203}$  and  $\text{Tl}^{205}$  Magnetic Resonance in Thallium and

- Thallic Oxide, *Phys. Rev.* **97**, 1679 (1955).
- [44] W. Hofstetter and T. Qin, Quantum simulation of strongly correlated condensed matter systems, *Journal of Physics B: Atomic, Molecular and Optical Physics* **51**, 082001 (2018).
- [45] S. Rachel, Interacting topological insulators: a review, *Reports on Progress in Physics* **81**, 116501 (2018).
- [46] S.-L. Yu, X. C. Xie, and J.-X. Li, Mott physics and topological phase transition in correlated Dirac fermions, *Phys. Rev. Lett.* **107**, 010401 (2011).
- [47] D. Cocks, P. P. Orth, S. Rachel, M. Buchhold, K. Le Hur, and W. Hofstetter, Time-Reversal-Invariant Hofstadter-Hubbard Model with Ultracold Fermions, *Phys. Rev. Lett.* **109**, 205303 (2012).
- [48] J. C. Budich, B. Trauzettel, and G. Sangiovanni, Fluctuation-driven topological Hund insulators, *Phys. Rev. B* **87**, 235104 (2013).
- [49] M. Potthoff and W. Nolting, Surface metal-insulator transition in the Hubbard model, *Phys. Rev. B* **59**, 2549 (1999).
- [50] Y. Song, R. Wortis, and W. A. Atkinson, Dynamical mean field study of the two-dimensional disordered Hubbard model, *Phys. Rev. B* **77**, 054202 (2008).
- [51] M. Snoek, I. Titvinidze, C. Töke, K. Byczuk, and W. Hofstetter, Antiferromagnetic order of strongly interacting fermions in a trap: real-space dynamical mean-field analysis, *New Journal of Physics* **10**, 093008 (2008).
- [52] M. Hafez-Torbati and W. Hofstetter, Artificial SU(3) spin-orbit coupling and exotic Mott insulators, *Phys. Rev. B* **98**, 245131 (2018).
- [53] M. Hafez-Torbati, D. Bossini, F. B. Anders, and G. S. Uhrig, Magnetic blue shift of Mott gaps enhanced by double exchange, *Phys. Rev. Research* **3**, 043232 (2021).
- [54] M. Hafez-Torbati, F. B. Anders, and G. S. Uhrig, Simplified approach to the magnetic blue shift of Mott gaps, *Phys. Rev. B* **106**, 205117 (2022).
- [55] M. Caffarel and W. Krauth, Exact diagonalization approach to correlated fermions in infinite dimensions: Mott transition and superconductivity, *Phys. Rev. Lett.* **72**, 1545 (1994).
- [56] S. Yunoki, J. Hu, A. L. Malvezzi, A. Moreo, N. Furukawa, and E. Dagotto, Phase Separation in Electronic Models for Manganites, *Phys. Rev. Lett.* **80**, 845 (1998).
- [57] R. Peters and T. Pruschke, Relevance of quantum fluctuations in the Anderson–Kondo model, *New Journal of Physics* **8**, 127 (2006).
- [58] Y. Motome and N. Furukawa, Monte carlo study of doping change and disorder effect on double-exchange ferromagnetism, *Phys. Rev. B* **68**, 144432 (2003).
- [59] X. Wang, E. Gull, L. de’ Medici, M. Capone, and A. J. Millis, Antiferromagnetism and the gap of a Mott insulator: Results from analytic continuation of the self-energy, *Phys. Rev. B* **80**, 045101 (2009).
- [60] Q. Niu, D. J. Thouless, and Y.-S. Wu, Quantized Hall conductance as a topological invariant, *Phys. Rev. B* **31**, 3372 (1985).
- [61] K. Ishikawa and T. Matsuyama, A microscopic theory of the quantum Hall effect, *Nuclear Physics B* **280**, 523 (1987).
- [62] Z. Wang, X.-L. Qi, and S.-C. Zhang, Topological Order Parameters for Interacting Topological Insulators, *Phys. Rev. Lett.* **105**, 256803 (2010).
- [63] V. Gurarie, Single-particle Green’s functions and interacting topological insulators, *Phys. Rev. B* **83**, 085426 (2011).
- [64] Z. Wang and S.-C. Zhang, Simplified Topological Invariants for Interacting Insulators, *Phys. Rev. X* **2**, 031008 (2012).
- [65] A. Blason and M. Fabrizio, Unified role of Green’s function poles and zeros in correlated topological insulators, *Phys. Rev. B* **108**, 125115 (2023).
- [66] D. Zhu, M. Kheirkhah, and Z. Yan, Sublattice-enriched tunability of bound states in second-order topological insulators and superconductors, *Phys. Rev. B* **107**, 085407 (2023).
- [67] B. Irsigler, J.-H. Zheng, and W. Hofstetter, Interacting Hofstadter Interface, *Phys. Rev. Lett.* **122**, 010406 (2019).
- [68] Z.-L. Gu, K. Li, and J.-X. Li, Quantum cluster approach to the topological invariants in correlated Chern insulators, *New Journal of Physics* **21**, 073016 (2019).
- [69] W.-X. He, R. Mondaini, H.-G. Luo, X. Wang, and S. Hu, Phase transitions in the Haldane-Hubbard model, *Phys. Rev. B* **109**, 035126 (2024).
- [70] T. Mertz, K. Zantout, and R. Valentí, Statistical analysis of the Chern number in the interacting Haldane-Hubbard model, *Phys. Rev. B* **100**, 125111 (2019).
- [71] C. Wu, B. A. Bernevig, and S.-C. Zhang, Helical liquid and the edge of quantum spin Hall systems, *Phys. Rev. Lett.* **96**, 106401 (2006).
- [72] C. Niu, J. P. Hanke, P. M. Buhl, G. Bihlmayer, D. Wortmann, S. Blügel, and Y. Mokrousov, Quantum spin Hall effect and topological phase transitions in honeycomb antiferromagnets, (2017), [arXiv:1705.07035](https://arxiv.org/abs/1705.07035).
- [73] R. S. K. Mong, A. M. Essin, and J. E. Moore, Antiferromagnetic topological insulators, *Phys. Rev. B* **81**, 245209 (2010).
- [74] Y. Yang, Z. Xu, L. Sheng, B. Wang, D. Y. Xing, and D. N. Sheng, Time-reversal-symmetry-broken quantum spin Hall effect, *Phys. Rev. Lett.* **107**, 066602 (2011).
- [75] H. Li, L. Sheng, and D. Y. Xing, Connection of edge states to bulk topological invariance in a quantum spin Hall state, *Phys. Rev. Lett.* **108**, 196806 (2012).
- [76] H. Li, L. Sheng, R. Shen, L. B. Shao, B. Wang, D. N. Sheng, and D. Y. Xing, Stabilization of the quantum spin Hall effect by designed removal of time-reversal symmetry of edge states, *Phys. Rev. Lett.* **110**, 266802 (2013).
- [77] W. Luo, D. X. Shao, M.-X. Deng, W. Y. Deng, and L. Sheng, Time-reversal-breaking induced quantum spin Hall effect, *Scientific Reports* **7**, 43049 (2017).
- [78] Z. Wang, X. Wang, Z. Hu, D. Bongiovanni, D. Jukić, L. Tang, D. Song, R. Morandotti, Z. Chen, and H. Buljan, Sub-symmetry-protected topological states, *Nature Physics* **19**, 992 (2023).
- [79] D. Bossini, M. Terschanski, F. Mertens, G. Springholz, A. Bonanni, G. S. Uhrig, and M. Cinchetti, Exchange-mediated magnetic blue-shift of the band-gap energy in the antiferromagnetic semiconductor MnTe, *New Journal of Physics* **22**, 083029 (2020).